Volume 14, Issue 4, 142446 (1-10)

Iranian Journal of Catalysis (IJC)

https://doi.org/10.57647/j.ijc.2024.1404.46

Catalytic activity of nickel doped rutile in oxygen reduction reaction (ORR) of proton exchange membrane fuel cell (PEMFC): a potential nuclear magnetic resonance (NMR) based investigation

Marufuzzaman[1], Md Abdus Salam[1,2,*], Robert Steinberger-Wilckens[3]

[1]*Hydrogen Energy Laboratory, BCSIR Laboratories Chattogram, Bangladesh.*
[2]*IMMM, BCSIR, Joypurhat, Bangladesh.*
[3]*School of Chemical Engineering, College of Engineering and Physical Sciences, University of Birmingham, United Kingdom.*

[*]**Corresponding author:** salam.bcsir1@gmail.com

Original Research

Received:
17 July 2024
Revised:
6 October 2024
Accepted:
1 November2024
Published online:
16 November 2024

Abstract:

The immense deployment trend of proton exchange membrane fuel cells (PEMFC) globally to the power generation and automobile industries grows massive technological development to make it efficient and sustainable. Oxygen reduction reaction (ORR) plays a key role in making efficient of PEMFC. Nuclear magnetic resonance (NMR) based investigation able to predict the cost-effective replacement of potential oxygen reduction reaction (ORR) catalyst for proton exchange membrane fuel cell (PEMFC). Nickel-doped (1%) rutile demonstrates better and substantial electrochemical activity toward ORR. Rutile and Pt, Pd, and Ni-doped rutiles are subjected to NMR and nuclear quadrupole resonance (NQR) analyses using CASTEP and Gaussian computational code to find the charge density effect of Platinum, Palladium, and Nickel on the titanium and oxygen atoms of rutile. The chemical shifts of titanium, Ti (6) of Platinum, Palladium, and Nickel-doped rutile are −1621, −4037, −5127 and 7823. The in-depth analyses show that Platinum, Palladium, and Nickel dopants to the rutile increase the electron density and electric conductivities as well as the overall catalytic performance due to the structural defects, creating oxygen vacancy and Ti^{3+} that favor the ORR reaction. The EFG Tensor, Eta (η), NQCC, shielding tensor corresponds that Ni is a better doping element among three (Pt, Pd & Ni) in rutile for ORR catalyst of PEMFCs.

Keywords: NMR; Rutile; Doping; EFG; NQCC; Shielding

1. Introduction

The fuel cell is one of the most promising energy conversion technologies since it is an electrochemical device that directly transforms chemical energy into electrical energy with minimal environmental impact. Fuel cells have attracted the interest of researchers and businesses over the past couple of years as cutting-edge electrical energy conversion technology. Proton exchange membrane fuel cells (PEMFCs) are viewed as the most important conversion technologies due to the good number of sources, zero emissions, instant startup, and high productivity [1–4]. The deployment of proton exchange membrane fuel cells (PEMFCs) is rapidly increasing as a source of stationary power and automotive applications. Nowadays, fuel cell vehicles such as buses, cars, forklifts, and trains are in the market launched by Toyota, Honda, and Hyundai. The internal combustion engine and batteries are more competitive than

PEMFCs, though the modern fuel cell stack shows a significant power density of 6 kWL^{-1}, low-temperature operation, compactness, low weight, low cost & volume, fast start-ups, and discontinuous operation facilities. End-user cost and lifetime of cells are crucial issues in this regard to consider. Advancements in technologies and materials and the scale-up of production are required to improve the membrane electrode assembly (MEA) of the heart of PEMFCs. Integrating with traditional power generation systems or distributing on-site power systems has been explored. Moreover, its diverse application to the agricultural and industrial sectors is the additional focus shortly. Some chronological development changes in the structure of fuel cells make them identical in the operation and conditions of the cells [5–8].

The basic working principle of PEMFC is that hydrogen is supplied to the anode as a fuel, and air or oxygen (Oxidant) is supplied to the cathode to complete the energy conversion reaction. Hydrogen splits into protons and electrons at the anode, and electrons pass through the outer circuit to the electric load. Secondly, proton transfer through the membrane (electrolyte) and react with oxygen at the cathode. An active catalyst enhances both of the reactions. Efficient oxygen reduction plays a major role in PEMFC operation. Before PEMFC's commercialization, there are still a lot of obstacles to overcome. An active and affordable catalyst for the oxygen reduction process is one of them (ORR) to solve the limitation. Oxygen reduction follows two different reaction paths: reduction by 4 (four) electrons, where it forms oxygen (O_2) and water (H_2O), and reduction by 2(two) electrons that form Oxygen (O_2) and hydrogen peroxide (H_2O_2). 4 (four) electrons reduction considered as the favorable path due to the absence of hydrogen peroxide formation. The path creates some degradation of the membrane and electrode. As a result, the operating potential and current density become high in fuel cells [9–12]. Oxygen reduction reaction (ORR) occurs by moving a four-electron in one step, as shown in Equ. (1) and by moving two electrons in two steps, as shown in Equ. (2) [13].

$$O_2 + H_2O + 4e^- \rightarrow 4OH^- \quad (1)$$

$$O_2 + H_2O + 2e^- \rightarrow OH^- + HO_2^- \quad (2)$$

$$H_2O + HO_2^- + 2e^- \rightarrow 3OH^-$$

There is a challenge to the oxygen reduction rate at the cathode of PEMFC. A good number of efforts have been made to accelerate the ORR in fuel cells. The most well-known catalysts for the oxygen reduction reaction are gold, ruthenium, palladium, platinum, and their alloys [14], as well as carbon-based materials, i.e., N-doped carbon nanotubes, N-doped graphene, sulfur-doped graphene [15–20]. The noble metals are expensive, and consequently, the main challenge is to decrease or replace Pt and Pt-based alloy catalysts in ORR reactions [21].

According to the literature regarding the reduction state, an associative mechanism occurs for water adsorption and dissociative formation at bridging oxygen vacancies. It is a common defect on the surface of rutile and rutile-making hydroxyl groups for linking with atoms. It has been well studied that the oxygen (O_2) adsorption in the first step of oxygen reduction reaction and the presence of bridging -OH on a rutile surface. Hydrogen peroxide and adsorbed OOH showed the most stable formation or transition state due to the surrounding bridging OH and the hydrogen bonds that make them the most stable [22, 23]. Week intermediates are O_2 and H_2O or OH, which are not supported by calculation. Oxygen and neighboring *OH* groups spontaneously form the OOH species adsorbed on the surface [24]. The formation of a bond between OOH and titanium is necessary for the four-electron method, and OOH reacts with titanium atoms with a lower charge density. As a result, the charge density of titanium atoms in the studied rutile is a criterion for OOH attack. Titanium atoms with lower charge densities react more easily with OOH. [25]

Nuclear quadrupole resonance (NQR) spectroscopy is a highly sensitive method for measuring the electronic charge distribution around quadrupole nuclei [26]. This method enables us to find out more about specific quadrupole nucleus surroundings to determine the electronic structure of molecules and complexes. Moreover, it can assess the EFG of the molecule's charges at any point within the molecular space. The nuclear quadrupole coupling constant (NQCC) measures the interaction between the EFG and the quadrupole moment of the quadrupole nuclei.

Rutile is a low-cost, stable, and eco-friendly superconducting material that is electrically insulating at temperatures below 200 °C and is not a good replacement as a catalyst for ORR [27–29]. A good number of efforts have been made to enhance electronic conductivity to improve rutile electrochemical activities. Metals doping to the rutile is one of them that brings structural defects and oxygen vacancies [30, 31] and improves electrical conductivity (donor density) as well as electro-catalytic performances. Nickel (Ni), an abundant and reasonably priced element with favorable electrochemical characteristics, is a common element on Earth. It is used as an alternative or a co-catalyst in Pt-based materials of PEMFCs [32]. Rutile doped by Pt, Pd, and Ni shows significant electrochemical activity compared to Pt supported by conventional carbon [33, 34]. Pt, Pd, and Ni-doped rutiles are some of the most significant substitute catalysts.

The titanium atoms are six or five-fold coordinated on the rutile surface. Again, the oxygen (O) atoms are 3-fold coordinated in the surface plane or 2-fold coordinated with connecting atoms that come through from the surface [31, 35]. A couple of studies have been conducted on the properties of rutile surfaces [33, 34], especially the adsorption of water or oxygen [36–40] like small molecules. The catalytic activity of Pt, Pd & Ni-doped rutile on the ORR in PEMFCs has not been studied yet using NMR techniques. In this work, the doping effect of Pt, Pd & Ni on the rutile catalytic activities or performances, especially the charge density and oxygen vacancy phenomena that predict the ORR performances, was studied using the CASTEP and Gaussian computational code-based NMR analyses. Moreover, the parameters, i.e., shielding tensor, NQCC, and EFG, support the interpretation and selection of the best and most cost-effective ORR catalyst as a replacement for an expensive catalyst.

2. Materials and methods

The supercell approach was used for the first-principle electronic structure calculations of rutile and doped rutile. Pt-rutile, Pd-rutile, and Ni-rutile are built using the DFT-based DMol^3 module by doping Pt, Pd, and Ni in the pure rutile crystal structure. Geometrical optimization of the doped rutile crystals was performed using the DNP basis set and PBE (GGA) functional [41–43]. The geometrical optimization is performed at the conditions of −21336 Ha energy and 50 SCF iterations. The geometrically optimized crystal structure of rutile, Pt-rutile, Pd-rutile, and Ni-rutile are then subjected to NMR analyses using CASTEP computational code. The GGA/PBE computational model applied in the CASTEP module is a reliable computational code for calculating NQCC tensors [44]. The energy calculation of the geometrically optimized crystal structures was performed by OTFG ultra-soft pseudopotentials in the CASTEP module, where the energy cutoff (489.8 eV), K-point set ($2 \times 3 \times 2$), and fine SCF tolerance are maintained as electronic parameters. The successful NMR analyses provide the parameters: electric field gradient (EFG), shielding tensor, nuclear quadrupole coupling constants (NQCC), and EFG tensor (η that are used later in the results and discussion section to interpret the electronic phenomena of the catalyst. Moreover, NMR analyses of all investigated catalysts were performed again using Gaussian 09W computational code to observe the chemical shifts and related parameters as the pathways shown in Fig. 1.

The charge density of atoms in a molecule can be calculated by the nuclear magnetic resonance (NMR) using the CASTEP computational code [45]. The chemical shielding tensor σ_{mn} is obtained according to Eq. (3) as calculated by CASTEP where the nuclear magnetic moment (μ) and nuclear magnetic shielding (B) and the magnetic field is oriented in the m direction, and the shielding in the n direction.

$$\sigma_{mn} = \left(\frac{\delta^2 E}{\delta \mu_m \delta B_n} \right)_{\mu, B=0} \tag{3}$$

In solution-state NMR, each nucleus often exhibits a chemical shift as an isotropic value due to fast molecule tumbling, which averages the shielding tensor's orientation-dependent component [46]. Eq. (4) computes the isotropic value of the major component of the shield.

$$\sigma_{iso} = \frac{\sigma_{11} + \sigma_{22} + \sigma_{33}}{3} \tag{4}$$

Using the results of subscript representshe reference atom and σ_p represents the investigated atom; [47].

$$\delta_p = \frac{\sigma_{p,ref} - \sigma_p}{1 - \sigma_{p,ref}} \approx (\sigma_{p,ref} - \sigma_p) \tag{5}$$

The charge density of a compound can be derived by using the bond angles of the compounds. The bond angles of a compound are calculated by the EFG tensor (η) which is expressed in Eq. (6). [48].

$$\cos\theta_\infty = \frac{1}{3}\left(1 - \frac{4}{1+\eta}\right) \tag{6}$$

3. Results and discussion

The geometrically optimized structures of Rutile (a), Platinum-Rutile (b), Palladium-Rutile (c), and Nickel-Rutile (c) were subjected to the computational code and analyzed as shown in Fig. 2. The charge distribution and

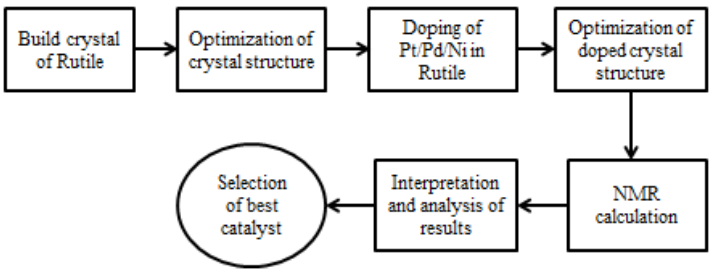

Figure 1. Method of investigation.

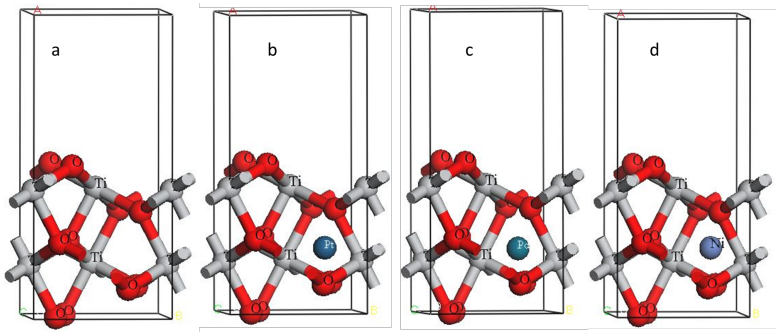

Figure 2. Rutile (a), Pt-Rutile (b), Pd-Rutile (c), and Ni- Rutile crstal.

ORR activities of titanium atoms in rutile and doped rutile's were analyzed and made comparison.

3.1 NMR analysis

The NMR spectrum of Rutile (a), Pt-Rutile (b), Pd-Rutile(c), Ni- Rutile (d) are shown in Fig. 3. The chemical shift (in ppm scale) of all atoms ranged in (+500 to −20000 ppm). It shows the effect of dopant Pt, Pd, and Ni atoms that alters the chemical shift of titanium and oxygen atoms in rutile.
The average chemical shifts (ppm) of titanium atoms in Rutile, Pt-Rutile, Pd-Rutile, and Ni-Rutile are shown in Table 1: −617 ppm, −2101 ppm, −2419 ppm, and −3091 ppm, respectively. Ni-Rutile has a wider chemical shift (ppm), which indicates the least charge density and is more active towards oxygen reduction reaction. The order of the catalysts towards ORR reactivity is likely Ni-rutile > Pd-rutile > Pt-rutile > rutile.
The chemical shifts (ppm) of titanium atoms in rutile (a), Pt-rutile (b), Pd-rutile(c), and Ni-rutile (d) are shown in Fig. 4, and their chemical shift (ppm) varied in the range of −200 to −8000 ppm.
NMR graph of doped atom in Pd-rutile, Pt-rutile, and Ni-rutile is shown in Fig. 5. The chemical shift (ppm) of platinum atom in Pt-Rutile is −432 ppm, palladium atom in Pd-Rutile is −566 ppm, and nickel atom in Ni-Rutile is −15842 ppm respectively as shown Fig. 5. The chemical shifts (ppm) of single platinum, palladium, and nickel atoms are −4186 ppm, −6496 ppm and −21758 ppm respectively shown in Fig. 5.
These doping elements cause the titanium atoms to shift higher and become a lower chemical shift itself, which lowers the charge density of titanium atoms in a rutile structure. Ni-rutile has more chemical shift (ppm), which indicates it has the least charge density and is more active toward oxygen reduction reaction. The order of the catalysts in ORR reactivity is likely Ni-rutile > Pd-rutile > Pt-rutile > Rutile. The more electronegative the neighbor, the greater the effect. An inductive effect drives the shift of NMR. The effect of electronegativity is additive. The more or less electron density present, the further upfield/downfield the shift in the spectrum. Electrons in the neighboring atoms could reduce the field experienced by the proton, shielding it from the external magnetic field and moving the signal to lower ppm (or upfield) and vice versa. The chemical shift values present a wider shift according to the decreasing metal charge in the order of Ni > Pd > Pt due to the coordinated shorter distance between the metal center and dopants, and a more covalent nature might occur with the increases of metal atomic number [49]. The larger shift corresponds to the reduction of metal ion charges upon going from Ni to Pd and finally to Pt. Only the level of dopant concentration is not a key reason to have a greater chemical shift (CS). Moreover, metal-ligand covalency and metal ion electron

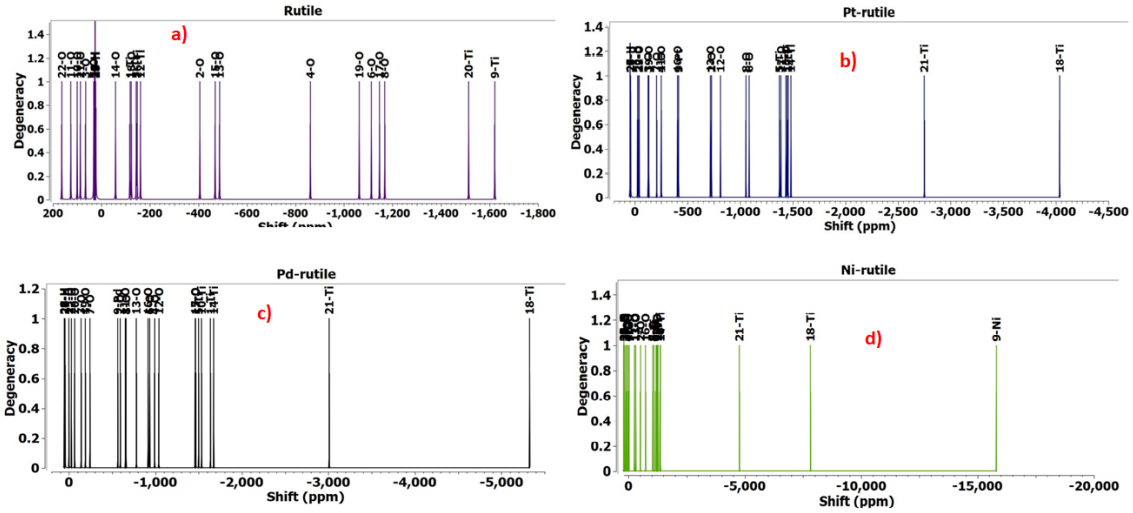

Figure 3. NMR graph of Rutile (a), Pt-Rutile (b),Pd-Rutile (c) and Ni-Rutile(d).

Table 1. Chemical Shifts/ δ_p (ppm) of titanium in rutile, Pt-Rutile, Pd-Rutile, and Ni-Rutile.

	Rutile	Pt-rutile		Pd-rutile		Ni-rutile	
Atom	δ_p (ppm)	Atom	δ_p (ppm)	Atom	δ_p (ppm)	Atom	δ_p (ppm)
Ti(1)	-117	Ti(1)	-1387	Ti(1)	-1461	Ti(1)	-1258
Ti(2)	-143	Ti(2)	-1460	Ti(2)	-1495	Ti(2)	-1429
Ti(3)	-147	Ti(3)	-1469	Ti(3)	-1593	Ti(3)	-1510
Ti(4)	-161	Ti(4)	-1496	Ti(4)	-1628	Ti(4)	-1529
Ti(5)	-1514	Ti(5)	-2758	Ti(5)	-2908	Ti(5)	-4895
Ti(6)	-1621	Ti(6)	-4037	Ti(6)	-5127	Ti(6)	-7923

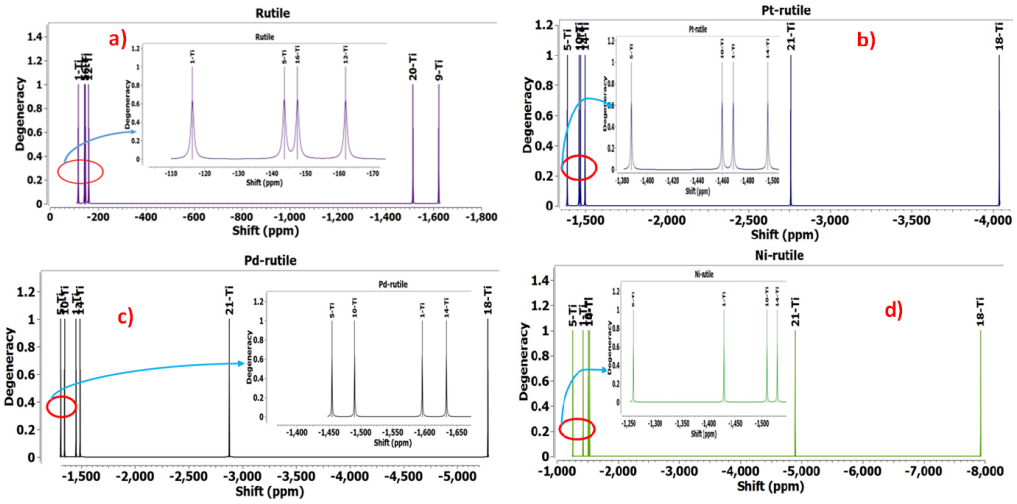

Figure 4. Chemical shift of titanium atoms (1 to 6) in Rutile (a), Pt-Rutile(b), Pd-Rutile(c), and Ni-Rutile(d).

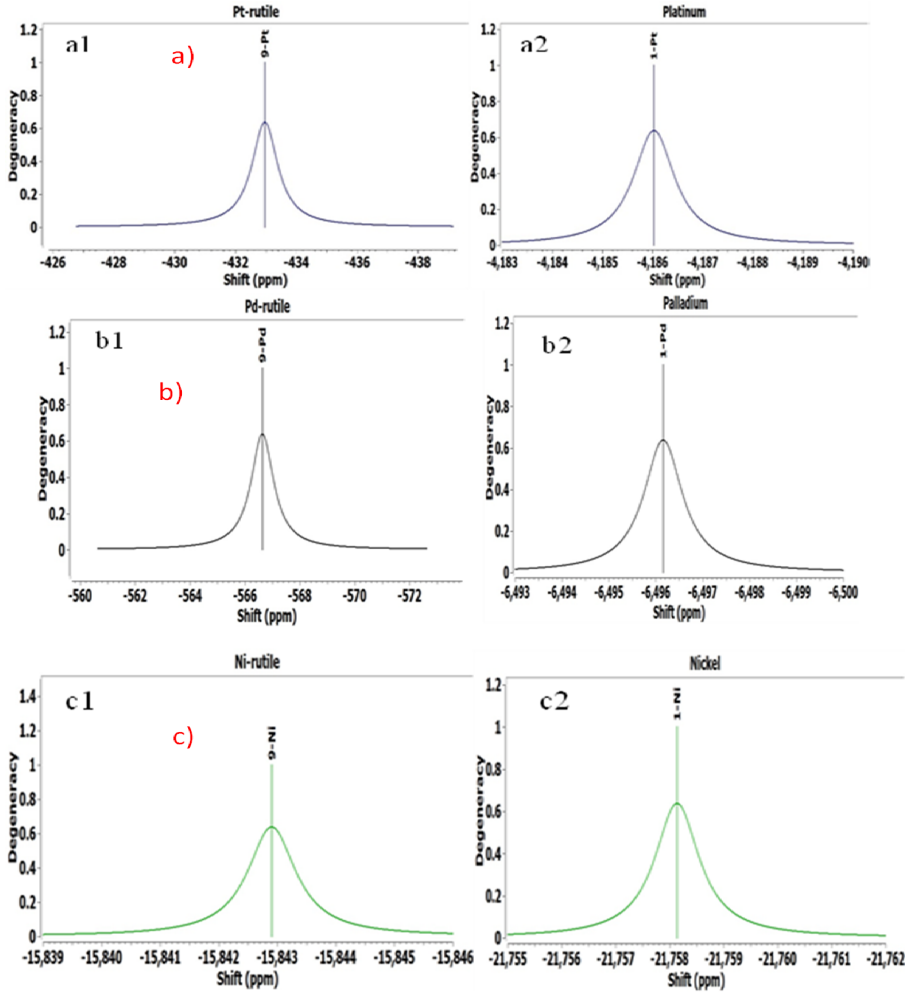

Figure 5. Chemical shift of Pt, Pd & Ni in Rutile (a1, b1, c1) and individual chemical shift of Pt, Pd & Ni (a2, b2, c2).

density affect the electron density of the nearest neighboring nuclei and subsequently affect the CS. Adsorption energies of oxygen and hydroxyl ions together with linear scaling relation are considered as ORR descriptors. Metals that bind with O and OH more strongly are less active. The addition of Nickel as a dopant weakens the bonding to ORR intermediates that favor the reaction. Further extensive DFT calculation is required to measure the optimal contents of dopant metal to maximize the ORR. The study focuses based on the structure-activity relation of molecules. The appearance of anatase titanium dioxide is metallic and has low relative density. Rutile titanium dioxide is optically

positive, and the degree of distortion of the octahedron is different and favors the metal doping that makes it good for ORR catalyst.

3.2 EFG tensors (η)

The comparison of bond angle for the Rutile, Pt-Rutile, Pd-Rutile, and ni-rutile can be observed by Eq. (6), which is applied for the bond angle calculation of O-Ti-O from the EFG Tensor, η in the range of ($109.47 < \theta_\infty < 180$) [50]. The angles of O-Ti-O in rutile and Pt/Pd/Ni-doped rutile are calculated by Eq. (6). In the case of rutile and Pt/Pd/Ni-doped rutile, titanium atoms that are connected with covalent bonds to the oxygen crystal lattice, the angles O-Ti-O depend on the geometry of the lattice. Moreover, O-Ti-O bond angles in rutile will give the charge density of titanium atoms. The O-Ti-O bond angles are calculated from the EFG tensors (η) in Table. 2 by solving Eq. (6).
The numerical decrease in the amount of EFG Tensor(η) indicates the numerical increase in the $\cos\theta_\infty$ indicating that these atoms have lower charge density [51]. The presence of Pt atoms in Pt-rutile has reduced the EFG Tensor(η) at titanium atom nunumbersf 2, 3, 5 ,and 6; Pd atoms in Pd-rutile have reduced the EFG Tensor (η) at titanium atom number of 2, 4, 5 and 6; and Ni atoms in Ni-rutile has reduced the EFG Tensor (η) at titanium atom number of 2, 3, 4, 5 and 6; The numerical value of EFG Tensor (η) decrease indicates the increase of $\cos\theta_\infty$ corresponds that these atoms have lower charge density. The bond angle study demonstrates that the titanium atom at Ni-rutile has a lower charge density than rutile. This lowest charge density makes the Ni-rutile catalyst more active towards ORR than rutile, Pt-rutile, and Pd-rutile. The EFG Tensor (η) analysis shows that Ni is a suitable doping element of Ni-rutile for proton exchange membrane fuel cells (PEMFCs) catalysts.

3.3 Shielding tensor

The shielding tensors of titanium and oxygen atoms in rutile, Pt-rutile, Pd-rutile, and Ni-rutile are obtained from NMR analyses using CASTEP computational codes. Six (6) titanium atoms named Ti(1), Ti(2), Ti(3), Ti(4), Ti(5), and Ti(6) of a rutile plane are studied for the selection of comparatively most active sites of the catalyst and tabulated in Table 3.
NMR analyses predict the shielding tensors of rutile, Pt-rutile, Pd-rutile, and Ni-rutile, which are shown in Table 3. It corresponds to the trend of the chemical shift of the investigated catalysts and the charge density of the titanium. Chemical shifts of rutile, Pt-rutile, Pd-rutile, and Ni-rutile are shown in Fig. 4. The chemical shifts of Ti (6) are; Rutile (1621), Pt-Rutile (4037), Pd-Rutile (5127), and Ni-Rutile (7923) as in Table 1. Ni-rutile shows the highest chemical shift than Pt and Pd-rutile. Higher chemical shifts corre-

Table 2. EFG tensor (η) of titanium in Pt, Pd, Ni-doped Rutile.

Nucleus Species	Bond angles of O-Ti-O in catalysts $\cos\theta_\infty$			
	rutile	Pt-rutile	Pd-rutile	Ni-rutile
Ti(1)	122.2	115.9	116.8	122.2
Ti(2)	126.3	128.7	128.7	127.8
Ti(3)	123.7	125.4	116.8	125.0
Ti(4)	124.6	118.3	129.2	125.9
Ti(5)	121.6	122.9	124.4	126.3
Ti(6)	122.9	126.3	127.8	128.7
Eta (η)/EFG Tensor values				
Ti(1)	0.54	0.73	0.70	0.54
Ti(2)	0.44	0.39	0.39	0.41
Ti(3)	0.50	0.46	0.70	0.47
Ti(4)	0.48	0.65	0.38	0.45
Ti(5)	0.56	0.52	0.49	0.44
Ti(6)	0.52	0.44	0.41	0.39

Table 3. EFG tensor (η) of titanium in Pt, Pd, Ni-doped Rutile.

Atom	Shielding tensor (Iso)			
	Rutile	Pt-rutile	Pd-rutile	Ni-rutile
Ti(1)	-436.25	-503.73	-520.46	-1717.49
Ti(2)	-465.32	-457.79	-576.84	-537.27
Ti(3)	-495.91	-535.51	-555.31	-565.31
Ti(4)	-434.48	-451.97	-584.70	-665.78
Ti(5)	-456.59	-487.21	-504.76	-567.56
Ti(6)	-493.16	-513.96	-546.84	-637.92

spond to the lower charge density [52] of the titanium of the rutile. The presence of each Pt, Pd & Ni atoms individually in rutile has reduced the charge density of the titanium atom from 1 to 6th. Increasing chemical shifts indicate the decrease of the charge density that favors the 4-electron reaction of ORR [53]. The analyses provide a competitive advancement on ORR catalyst that would be an active replacement of precious catalysts like Pt. Ni-doped rutile catalyst, which is a promising material for the future development of PEMFC.

3.4 NQCC

Fig. 6 indicates the Q_c (MHZ) of the titanium and oxygen atoms in Pt/Pd/Ni-doped rutile. The titanium atoms in Pt/Pd/Ni-doped rutile have lower Cq (MHZ) values than rutile. The calculated Q_c of oxygen atoms in Pt-rutile, Pd-rutile, and Ni-rutile was lower than that of O-atoms in Rutile, indicating that O-atoms in Pt-rutile, Pd-rutile, and Ni-rutile have a higher charge density than those in rutile. The calculated Q_c of titanium atoms in Pt-rutile, Pd-rutile, and Ni-rutile was higher than that of Ti-atoms in rutile, indicating that Ti-atoms in Pt-rutile, Pd-rutile, and Ni-rutile have a lower charge density than those in rutile. This condition makes the Pt/Pd/Ni-doped rutile more active toward the oxygen reduction reaction (ORR). Fig. 6 shows the QC of titanium atoms in Pt/Pd/Ni-doped rutile, which clearly expresses the order of reduced charge density in catalysts as Ni-rutile > Pd-rutile > Pt-rutile > Rutile.

4. Discussion

The kinetics of ORR is still a major challenge in the research and development of fuel cells. It would be possible to increase the efficiency of the fuel cell by creating better conditions of the reaction for easier four-electron methods in the OOR at the cathode. In the four-electron ORR mechanism, O-H is formed [54]

Doping Pt, Pd & Ni to the rutile increases the electron density and electric conductivities as well as the overall catalytic performance due to the structural defects and creates oxygen vacancy and Ti^{3+} [55–59]. The top view of the investigated catalyst is shown in Fig. 7. Reactive sites for the adsorption of oxygen and water have been hypothesized to exist in point defects [60–63]. Molecular oxygen adsorption has been reported to occur actively at the surface of oxygen vacancies. [64, 65]. In addition, oxygen vacancies have been proposed as active locations for water's dissociative adsorption. [66]. Then, hydrogen is adsorbed on a bridging lattice oxygen ion, and the OH group is adsorbed on an oxygen vacancy, filling the vacancy with an oxygen ion. [67] OH interacts with rutile (as a catalyst), where a chemical bond between oxygen and titanium is created. This is the most important step of the catalytic effect of rutile [59, 62]. The formation of the bond between OH and Ti is necessary for the four-electron method, and OH reacts with titanium atoms with a lower charge density. The charge density of titanium and oxygen atoms in rutile, Pt-rutile, Pd-rutile, and Ni-rutile are obtained from the numerical values of chemical shift shown in Eq. (5). Catalytic PEM has a high potential to add a versatile application towards clean energy [68].

The above discussion of the EFG tensor (η) indicates that the Ni-rutile catalyst is more active towards ORR than rutile, Pt-rutile, or Pd-rutile. From the NQCC study, the presence of Ni atoms in Ni-rutile causes the charge density of titanium atoms to decrease, and therefore, titanium atoms in Ni-rutile are more reactive in the four-electron path mechanism in the ORR reaction at the cathode. Finally, the EFG shielding tensor indicates Ni-rutile has a reduced charge density and increased chemical shifts. Ni-rutile's catalytic effect will be greater than pure rutile, Pt-rutile, and Pd-rutile. Therefore, the presence of Pt, Pd, and Ni atoms in the rutile decreases the charge density of titanium atoms. As a result, these atoms are more reactive in the four-electron path mechanism in the ORR reaction.

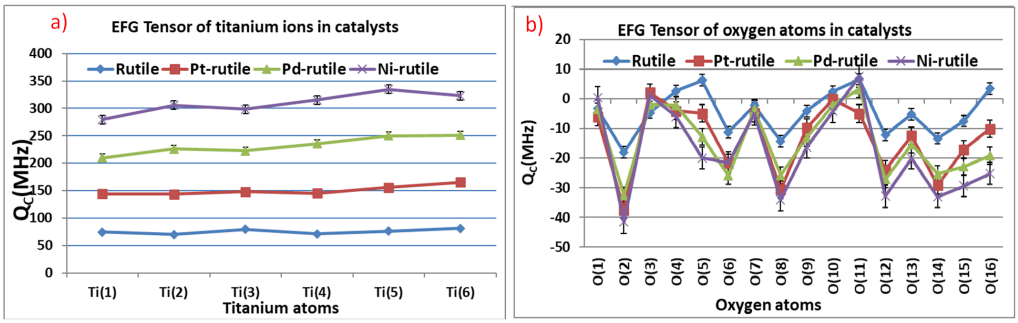

Figure 6. Comparative nuclear quadrupole coupling constant (Q_c)/MHZ of atoms in catalysts; (a) titanium, (b) Oxygen.

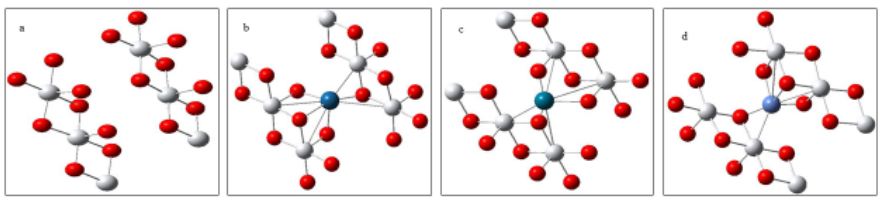

Figure 7. Top view of (a) rutile, (b) Pt-rutile, (c) Pd-rutile, (d) Ni-rutile in Gauss View in Gaussian NMR analysis.

5. Conclusion

The charge distributions are utilized to estimate the NMR and NQR parameters, which are used to comprehend the substance's electronic structures. The presence of Pt, Pd, and Ni in rutile decreases the charge density in titanium atoms and increases the charge density in oxygen atoms. The decreased charge density in titanium atoms makes the Pt, Pd, and Ni-doped rutile material more active than pure rutile. EFG tensors correspond to the Ni-Rutile, which is more active than rutile, Pt-rutile, and Pd-rutile towards ORR. Moreover, the nuclear quadrupole coupling constant (Q_c) predicts the titanium atoms in Pt, Pd, and Ni-doped rutile have a lower charge density than the rutile. Finally, from Gaussian NMR analysis, the numerical decrease in the amount of calculated chemical shielding Iso (ppm) indicates that the titanium atoms in Pt, Pd, and Ni-doped rutile catalysts have greater chemical shifts than pure rutile and the activity of Pt, Pd, Ni-doped rutile catalyst for ORR is likely Ni-rutile > Pd-rutile > Pt-rutile > Rutile. Increasing chemical shifts decrease the charge density of titanium, which means that they are suitable targets as the intermediate in the 4-electron reaction of ORR, which is a clear indication that the catalytic effect of Ni-rutile is greater than that of pure rutile, Pt-rutile, and Pd-rutile.

Acknowledgment
Hydrogen Energy Laboratory, Bangladesh Council of Scientific and Industrial Research (BCSIR) is the place where all the computational and analyses were performed. The authors are grateful to MoST, the Government Republic of Bangladesh, and the School of Chemical Engineering, College of Engineering and Physical Sciences, University of Birmingham, United Kingdom providing the required support.

Authors contributions
Authors have equally contributed in preparing the paper.

Availability of data and materials
The data that support the findings of this study are available from the corresponding author upon reasonable request.

Conflict of interests
The authors declare that they have no conflict of interest to be declared.

References

[1] W.R.W. Daud, R.E. Rosli, E.H. Majlan, S.A.A. Hamid, R. Mohamed, and T. Husaini. *Renew. Energ.*, **113C**(2017):620–638. DOI: https://doi.org/10.1016/j.renene.2017.06.027.

[2] J. Larminie, A. Dicks, and M.S. McDonald. *J. Wiley.*, **2**(2003):207–225.

[3] Y. Wang, D.F.R. Diaz, K.S. Chen, Z. Wang, and X.C. Adroher. *Mater Today.*, **32**(2020):178–203, . DOI: https://doi.org/10.1016/j.mattod.2019.06.005.

[4] F. Barbir. *PEM fuel cells*, (2012).

[5] H. Medetalibeyoglu, S. Manap, O. Aktas, M. Beytur, F. Kardas, O. Akyildirim, V. Ozkan, H. Yuksek, M.L. Yola, and N. Atar. *J. Electrochem. Soc.*, **165**(2018): F338. DOI: https://doi.org/10.1149/2.1041805jes.

[6] O. Akyildirim, H. Yuksek, and H. Saral. *J Mater Sci*, **27**(2016):8559–8566, . DOI: https://doi.org/10.1007/s10854-016-4873.

[7] B.G. Gunestekin nad H. Medetalibeyoglu, N. Atar, and M.L. Yola. *Electroanalysis*, **32**(2020):1977–1982. DOI: https://doi.org/10.1002/elan.202060074.

[8] O. Akyildirim, G. Kotan, M.L. Yola, T. Eren, and N. Atar. *Ionics*, **22**(2016):593–600, . DOI: https://doi.org/10.1007/s11581-015-1572-2.

[9] R.M. Felix-Navarro, M. Beltran-Gastelum, E.A. Reynoso-Soto, F. Paraguay-Delgado, G. Alonso-Nunez, and J.R. Flores-Hernandez. *Renew. Energ.*, **87**(2016):31–41. DOI: https://doi.org/10.1016/j.renene.2015.09.060.

[10] S. Chen and A. Kucernak. *J. Phys. Chem. B.*, **108**(2004):3262–3276. DOI: https://doi.org/10.1021/jp036831j.

[11] M.J. Janik, C.D. Taylor, and M. Neurock. *J. Electrochem. Soc.*, **156**(2008):B126. DOI: https://doi.org/10.1149/1.3008005.

[12] D. Eberle and B. Horstmann. *Electrochim. Acta.*, **137**(2014):714–720. DOI: https://doi.org/10.1016/j.electacta.2014.05.144.

[13] M.N. Sweety and M.A. Salam. *Chinese Journal of Chemical Engineering.*, **74**(2024):100–116. DOI: https://doi.org/10.1016/j.cjche.2024.06.011.

[14] J. Smith, L. Johnson, K. Lee, M. Wang, and R. Martinez. *J. Electrochem. Catal.*, **20**(2021):300–325. DOI: https://doi.org/10.1016/j.jelecat.2021.04.009.

[15] L. Yang, S. Jiang, Y. Zhao, L. Zhu, S. Chen, X. Wang, Q. Wu, J. Ma, Y. Ma, and Z. Hu. *Angew. Chem.*, **123**(2011):7270–7273, . DOI: https://doi.org/10.1002/anie.201101879.

[16] Z.H. Sheng, L. Shao, J. Chen, W. Bao, F.B. Wang, and X.H. Xia. *J. Mater. Chem.*, **22**(2012):390–395. DOI: https://doi.org/10.1039/C1JM13845A.

[17] Z. Yang, Z. Yao, G. Li, G. Fang, H. Nie, X. Zhou, X. Chen, and S. Huang. *ACS Nano.*, **6**(2011):205–211, . DOI: https://doi.org/10.1021/nn203393p.

[18] I.Y. Jeon, H.J. Choi, S.M. Jung, J.M. Seo, M.J. Kim, L. Dai, and J.B. Baek. *Adv. Mater.*, **25**(2013):6138–6145. DOI: https://doi.org/10.1002/adma.201302098.

[19] J. Wang, H. Tang, Y. Li, Z. Cui, Y. Wang, J. Yu, and J. Zhang. *Sci. Rep.*, **5**(2015):9304, . DOI: https://doi.org/10.1038/srep09304.

[20] Z. Ma, X. Dou, K. Dai, J. Dai, C. Li, J. Qiu, and L. Wang. *Angew. Chem. Int.*, **54**(2015):1888–1892. DOI: https://doi.org/10.1002/anie.201409869.

[21] M. Shao. *J. Power Sources.*, **196**(2011):2433–2444. DOI: https://doi.org/10.1016/j.jpowsour.2010.11.010.

[22] A.V. Bandura, D.G. Sykes, V. Shapovalov, T.N. Troung, J.D. Kubicki, and R.A. Evarestov. *J. Phys. Chem. B.*, **108**(2004):7844–7853. DOI: https://doi.org/10.1021/jp037466t.

[23] A. Ganyecz, P.D. Mezei, and M. Kallay. *Comput Theor. Chem.*, **1168**(2019):11260. DOI: https://doi.org/10.1016/j.comptc.2019.11260.

[24] A. Tilocca, C. Di Valentin, and A. Selloni. *J. Phys. Chem. B.*, **109**(2005):20963–20967. DOI: https://doi.org/10.1021/jp0531455.

[25] Y. Du, N.A. Deskins, Z. Zhang, Z. Dohnalek, M. Dupuis, and I. Lyubinetsky. *J. Phys. Chem. C.*, **113**(2009):666–671. DOI: https://doi.org/10.1021/jp808036k.

[26] B. H. Suits. *Nuclear quadrupole resonance spectroscopy*, (2006):65–96. DOI: https://doi.org/10.1007/978-0-387-26377-3_4.

[27] T. Ioroi, Z. Siroma, N. Fujiwara, S.I. Yamazaki, and K. Yasuda. *J. Iran. Chem. Soc.*, **7**(2005):183–188. DOI: https://doi.org/10.1016/j.elecom.2004.12.003.

[28] P. Clechet, C. Martelet, J.R. Martin, and R. Olier. *Electrochim. Acta.*, **24**(1979):457–461. DOI: https://doi.org/10.1016/0013-4686(79)87035-8.

[29] B. Parkinson, F. Decker, J.F. Juliao, M. Abramovich, and H.C. Electrochim. *Acta*, **25**(1980):521–525. DOI: https://doi.org/10.1016/0013-4686(80)87051-4.

[30] J. Li, H. Zhou, H. Zhuo, Z. Wei, G. Zhuang, X. Zhong, and J. Wang. *J. Mater. Chem.*, **6**(2018):2264–2272. DOI: https://doi.org/10.1039/C7TA09831F.

[31] M. Chisaka, Y. Yamamoto, N. Itagaki, and Y. Hattori. *ACS Appl. Energy Mater.*, **1**(2018):211–219. DOI: https://doi.org/10.1021/acsaem.7b00100.

[32] T. He, E. Kreidler, L. Xiong, and E. Ding. *J. Power Sources.*, **165**(2007):87–91. DOI: https://doi.org/10.1016/j.jpowsour.2006.12.030.

[33] J.M. Chen, L.S. Sarma, C.H. Chen, M.Y. Cheng, S.C. Shih, G.R. Wang, and B.J. Hwang. *J. Power Sources.*, **159**(2006):29–33. DOI: https://doi.org/10.1016/j.jpowsour.2006.04.135.

[34] N. Rajalakshmi, N. Lakshmi, and K.S. Dhathathreyan. *Int. J. Hydrog. Energy.*, **33**(2008):7521–7526. DOI: https://doi.org/10.1016/j.ijhydene.2008.09.032.

[35] U. Diebold. *Surf. Science. Rep.*, **48**(2003):53–229. DOI: https://doi.org/10.1016/S0167-5729(02)00100-0.

[36] X.Y. Pan, M.Q. Yang, X.Z. Fu, N. Zhang, and Y.J. Xu. *Nanoscale*, **5**(2013):3601–3614. DOI: https://doi.org/10.1039/C3NR00476G.

[37] G.M. Wang, Y.C. Ling, and Y. Li. *Nanoscale*, **4**(2012):6682–6691, . DOI: https://doi.org/10.1039/C2NR32222F.

[38] J. Nowotny. *Energy Environ. Sci.*, **1**(2008):565–572. DOI: https://doi.org/10.1039/B809111K.

[39] M. Xing, W. Fang, M. Nasir, Y. Ma, J. Zhang, and M. Anpo. *J. Catal.*, **297**(2013):236–243. DOI: https://doi.org/10.1016/j.jcat.2012.10.014.

[40] G. Liu, H.G. Yang, J. Pan, Y.Q. Yang, G.Q. Max Lu, and H.M. Cheng. *J. Phys. Chem. C*, **113**(2009):21784–21788. DOI: https://doi.org/10.1021/jp907749r.

[41] B. Delley. *J. Chem. Phys.*, **92**(1990):508–517, . DOI: https://doi.org/10.1063/1.458452.

[42] B. Delley. *J. Chem. Phys.*, **113**(2000):7756–7764, . DOI: https://doi.org/10.1063/1.1316015.

[43] D.A. Hanaor, M.H. Assadi, S. Li, A. Yu, and C.C. Sorrell. *Comput. Mech.*, **50**(2012):185–194. DOI: https://doi.org/10.1007/s00466-012-0728-4.

[44] M.A. Rafiee. *Int. j. phys. Sci.*, **28**(2017):69–79. DOI: https://doi.org/10.21315/jps2017.28.3.5.

[45] M. Maiwald, H.H. Fischer, Y.K. Kim, K. Albert, and H. Hasse. *J. Magn. Reson.*, **166**(2004):135–146. DOI: https://doi.org/10.1016/j.jmr.2003.09.003.

[46] J. Gauss and J.F. Stanton. *Adv Chem Phys.*, **123**(2002):355–422. DOI: https://doi.org/10.1002/0471231509.ch6.

[47] B. Adrjan, W. Makulski, K. Jackowski, T.B. Demissie, K. Ruud, A. Antusek, and M. Jaszunski. *Phys. Chem. Chem. Phys.*, **18**(2016):16483–16490. DOI: https://doi.org/10.1039/C6CP01781A.

[48] E. Kochanski, J.M. Lehn, and B. Levy. *Chem. Phys. Lett.*, **4**(1969):75–78. DOI: https://doi.org/10.1016/0009-2614(69)85072-4.

[49] N.M. Sanchez-Padilla, R. Benavides, C. Gallardo, S. Fernandez, E. De-Casas, and D. Morales-Acosta. *Int. J. hydrogen Energy*, **46**(2021):26040–26052. DOI: https://doi.org/10.1016/j.ijhydene.2021.03.023.

[50] U. Sternberg. *Solid State Nucl. Magn. Reson*, **2**(1993):181–190. DOI: https://doi.org/10.1016/0926-2040(93)90023-G.

[51] B. Jiang, J.M. Zuo, N. Jiang, M. O'Keeffe, and J.C.H. Spence. *Acta Crystallogr. A.*, **59**(2003):341–350. DOI: https://doi.org/10.1107/S010876730301122X.

[52] T.W. Keal and D.J. Tozer. *J. Chem. Phys.*, **19**(2003): 3015–3024. DOI: https://doi.org/10.1063/1.1590950.

[53] J. Zhang, Y. Yin, W. Zhang, H. Wang, X. Liu, J. Li, Z. Chen, H. Hu, Y. Wang, X. Zhu, and X. Zhou. *Electrochem. Ener. Rev.*, **6**(2023):15–58. DOI: https://doi.org/10.1007/s41918-022-00118-9.

[54] J.K. Norskov, J. Rossmeisl, A. Logadottir, L. Lindqvist, J.R. Kitchin, T. Bligaard, and H. Jonsson. *J. Phys. Chem. B.*, **108**(2004):17886–17892. DOI: https://doi.org/10.1021/jp047349j.

[55] R.L. Kurtz, R. Stock-Bauer, T.E. Msdey, E. Roman, and J.L. De Segovia. *Surf. Sci.*, **218**(1989):178–200. DOI: https://doi.org/10.1016/0039-6028(89)90626-2.

[56] G. Lu, A. Linsebigler, and J.T. Yates. *J. Chem. Phys.*, **102**(1995):3005–3008, . DOI: https://doi.org/10.1063/1.468609.

[57] G. Lu, A. Linsebigler, and J.T. Yates. *J. Phys. Chem.*, **102**(1995):4657–4662, . DOI: https://doi.org/10.1063/1.469513.

[58] M.A. Henderson. *Surf. Sci.*, **355**(1996):151–166. DOI: https://doi.org/10.1016/0039-6028(95)01357-1.

[59] M.A. Henderson, W.S. Epling, C.L. Perkins, C.H.F. Peden, and U. Diebold. *J. Phys. Chem. B*, **103**(1999): 5328–5337. DOI: https://doi.org/10.1021/jp990655q.

[60] M.P. de Lara-Castells and J.L. Krause. *Chem. Phys. Lett.*, **354**(2002):483–490. DOI: https://doi.org/10.1016/S0009-2614(02)00179-3.

[61] M. Menetrey, A. Markovits, and C. Minot. *Surf. Sci.*, **524**(2003):49–62. DOI: https://doi.org/10.1016/S0039-6028(02)02464-0.

[62] D. Vogtenhuber, R. Podloucky, and J. Redinger. *Surf. Sci.*, **402-404**(1998):798–801. DOI: https://doi.org/10.1016/S0039-6028(97)01083-2.

[63] S. Wendt, P.T. Sprunger, E. Lira, G.K.H. Madsen, Z. Li, J.O. Hansen, J. Matthiesen, A. Blekinge-Rasmussen, E. Laegsgaard, B. Hammer, and F. Besenbacher. *Science.*, **320**(2008):1755–1759. DOI: https://doi.org/10.1126/science.1159846.

[64] V.E. Henrich. *Prog. Surf. Science.*, **9**(1979):143–164. DOI: https://doi.org/10.1016/0079-6816(79)90011-X.

[65] W. Geopel, G. Rocker, and R. Feierabend. *Phys. Rev. B: Condens. Matter.*, **28**(1983):3427–3438. DOI: https://doi.org/10.1103/PhysRevB.28.3427.

[66] W.J. Lo, Y.W. Chung, and G.A. Somorjai. *Surf. Science.*, **71**(1978):199–219. DOI: https://doi.org/10.1016/0039-6028(78)90328-X.

[67] V.E. Henrich, G. Dresselhaus, and H.J. Zeiger. *J. Vac. Sci. Technol.*, **15**(1978):534–537. DOI: https://doi.org/10.1116/1.569464.

[68] M.A. Salam, K. Ahmed, M.N. Sweety, and P. Saha. *Int. J. hydrogen Energy*, **86**(2024):153–165. DOI: https://doi.org/10.1016/j.ijhydene.2024.08.343.